Molecular Crystals and Liquid Crystals

Publication details, including instructions for authors and subscription information:
http://www.tandfonline.com/loi/gmcl20

Surfactant Controlled Light Induced Reorientation in Dye-Doped Nematic Liquid Crystals

Stefania Residori [a], Grazia Russo [a], Sandra McConville [a] & Artyom Petrosyan [b]

[a] Institut Non Linéaire de Nice, Route des Lucioles, Valbonne, France

[b] Laboratoire de Physique de l'ENS-Lyon, Lyon, France

Version of record first published: 31 Aug 2006

To cite this article: Stefania Residori, Grazia Russo, Sandra McConville & Artyom Petrosyan (2005): Surfactant Controlled Light Induced Reorientation in Dye-Doped Nematic Liquid Crystals, Molecular Crystals and Liquid Crystals, 429:1, 111-132

To link to this article: http://dx.doi.org/10.1080/15421400590930791

Mol. Cryst. Liq. Cryst., Vol. 429, pp. 111–132, 2005

ISSN: 1542-1406 print/1563-5287 online
DOI: 10.1080/15421400590930791

Taylor & Francis
Taylor & Francis Group

Surfactant Controlled Light Induced Reorientation in Dye-Doped Nematic Liquid Crystals

Stefania Residori
Grazia Russo
Sandra McConville
Institut Non Linéaire de Nice, Route des Lucioles, Valbonne, France

Artyom Petrosyan
Laboratoire de Physique de l'ENS-Lyon, Lyon, France

We report new advancements in the experimental investigation of the giant optical nonlinearity observed in azo-dye doped nematic liquid crystals. We show that the extreme sensitivity of the azo-dye doped nematics results from a combined action of the trans-cis photoisomerization process of the azo-dye molecules and the light-induced changes of the anchoring energy. The molecular reorientation at the surface can be controlled by changing the length n of the aliphatic chain of the ionic surfactant, C_nTAB, used as anchoring agent. Polarization holography experiments show that, during the reorientation, the nematic director mainly follows the direction imposed by the linear polarization along the interference pattern. The diffraction gratings show a large response, proving that all the mechanisms related to light intensity gradients, such as charge migration or thermal heating, may be excluded from the effects that are at the origin of the giant nonlinearity.

Keywords: azo-dye doped nematic liquid crystals; giant optical nonlinearities; polarization holography; surface effects

INTRODUCTION

Giant amplification of the light-induced reorientation in dye-doped nematic liquid crystals with respect to the pure case has been reported in the case of the azo-dye Methyl Red (MR) in the liquid crystal 5CB

G. Russo benefits of a research fellowship (N° 575) of the French Ministry of Research. S. McConville had a grant for the Summer LPO Project (N° 200003166), Department of Physics, University of Strathclyde, UK.

Address correspondence to Stefania Residori, Institue non Lineaire de Nice, UMR 6618 CNRS_UNSA, 1361 Route des Lucioles, Valbonne, F-06560, France. E-mail: stefania.residori@inln.cnvs.fr

[1]. This was firstly interpreted as a photorefractive effect, due to optically induced charge migration in the sample [1]. Nevertheless, nowadays the more credited explanation is the one assuming light-induced modifications of the anchoring conditions at the confining surfaces of the cell [2]. In particular, we have recently shown that the extreme sensitivity of the azo-dye doped mixture is indeed mediated by the specific alignment agent used for surface anchoring treatment [3,4].

We report here further advancements in the field, through a systematic investigation on the influence of the surface conditions. We have performed different experiments by changing the length n of the aliphatic chain of the ionic surfactant, C_nTAB used as anchoring agent. We show that an extremely high sensitivity, recently referred to as a "colossal" optical nonlinearity [5], is obtained only when the surfaces are treated with a particular form of the surfactant, known as *hexadecyl trimethylammonium bromide, HTAB*, and corresponding to $n = 19$.

Another important experimental evidence comes from the role of the *trans-cis* photoisomerization of the azo-dyes when irradiated in their absorption band (laser wavelength $\lambda \sim 500\,\text{nm}$) [6]. When close to the surfaces, the molecular conformation change of the azo-dyes induces a reorientation of the nematic director, triggering the switching of the whole realignment in the bulk of the cell. In order to better account for the role of the photoisomerization, we have tested our best response cells ($n = 19$) for different concentrations of the dyes. Then, for a fixed and optimal dye concentration ($\simeq 0.3\%$ in weight), we give a detailed characterization of the dynamical diffraction gratings written by using a polarization holographic technique.

Polarization patterns are obtained by superposing two orthogonally polarized beams. At difference with the usual intensity holographic technique, an uniform intensity distribution is obtained in the interference region, while the resulting light polarization varies periodically from linear to elliptical, depending on the phase shift between the two interfering waves. Due to this property, when the cell is illuminated by polarization patterns, if a diffraction grating is formed in the sample, we can exclude the occurrence of phenomena that are due to intensity gradients, such as charge migration, temperature gradients and modulations of the dye concentration. Recently, high resolution permanent polarization gratings have been recorded in planar cells, showing an extremely high sensitivity of the mixture at the light polarization [7]. For the same system, it has also been shown that the main contribution to the refractive index change is the molecular reorientation rather than variations of the order parameter [8]. Here,

by testing our homeotropic cells we show the occurrence of dynamical gratings under illumination with polarization interference patterns.

When resuming all the results, obtained either for intensity or polarization interference patterns, both for linear and circular polarization of the pumps, by changing either the molecular length of the surfactant or the concentration of the azo-dye, we can conclude that surface and bulk contributions combine in such a way that the resulting reorientation of the director mainly follows the incident light polarization, leading to a stable grating formation. However, there are still many unanswered questions on the microscopic origin of the effect and a clear model able to establish an exact balance between the surface and bulk contributions to the whole reorientation process is still lacking.

In the first part of the article we present the methods for preparation of the homeotropic cells and we illustrate the alignment instability taking place, under light illumination, for some molecular lengths of the surfactant. Then, we describe the experimental setup and we discuss the results obtained for different molecular length of the ionic surfactant as well as for different concentration of the azo-dye. Finally, we discuss the experimental results and we suggest the possible mechanism which could be at the basis of the extreme sensitivity of the cell at the surface conditions. In the second part of the article, we present the polarization holography experiments, both for linearly and circularly polarized pumps, and we outline the role of photoisomerization of the dyes in the volume of the cell.

THE CELL PREPARATION AND THE ALIGNMENT INSTABILITY

All our cells are made by ITO coated glass plates (Asahi Glass). The size of each glass plate is $20 \times 30\,\mathrm{mm}^2$. The plates are cleaned in ultra-sound bath at $25^{\circ}C$ for 15–20 minutes with a Micro 90 cleaning solution (Bioblock Scientific). After cleaning, the slides are rinsed in a highly purified water ($R \simeq 18\,\mathrm{M}\Omega$) and then dried with filtered compressed air. The clean glass plates are then treated for deposition of the alignment agent. All the cells are filled with a mixture of the azo-dye Methyl Red, MR (Aldrich Chemicals), in the liquid crystal *p-n-pentyl-pcyanobiphenyl*, 5CB (Merck). The MR concentration c has been changed from $c = 0.1\%$ to $c = 1.0\%$ in weight. However, the best compromise between a large response and a low absorption has been found to be around $c = 0.3\%$, so that most of the experiments have been performed at this value of the MR concentration. Typical cell thickness is $d = 14\,\mu\mathrm{m}$. Before filling the cells, the azo-dye doped

liquid crystals are filtered, by centrifuging with 0.22 μm Millipore filters, as well as degassed in a vacuum oven [4].

To obtain the homeotropic alignment we have deposed a surfactant monolayer over the glass substrates [9]. We have used different surfactants of the same family C_nTAB, the general chemical formula is $C_nH_{2(n+1)}BrN$, where $(n-4)$ is the number of CH_2 groups in the aliphatic chain. The deposition of the C_nTAB mono-layer film was obtained by withdrawing the glass plates very slowly out of a water solution. The withdrawing speed was about 5 mm/min and typical concentration of surfactant was $\simeq 10^{-5}$ M. In Figure 1 it is shown a schematic drawing of the cell together with the chemical representation of the liquid crystal 5CB, of the azo-dye MR and of the surfactant used. In the figure we have represented the case $n = 19$, $C_{19}TAB$ or *HTAB*, *hexadecyl trimethylammonium bromide*, corresponding to the molecular compound more frequently used as anchoring agent [3,4]. In the same figure are shown the electric field E_0, resulting from the ionic distribution close to the surface and responsible of the anchoring force, the surface polarization P_s and the photo-induced field E_{PH}. Later, we will discuss in more detail the role of these fields, as well as their interplay leading to light-induced modifications of the anchoring energy.

We have prepared different cells, by treating the glass plates with different surfactants, varying n from 13 to 21 and also by changing the immersion times of the glass plates in the solution before the extraction. Once assembled, the cells were filled them with the mixture of liquid crystal and azo-dyes, 0.3% MR in 5CB. For all the cells, the final quality of the liquid crystal alignment was tested

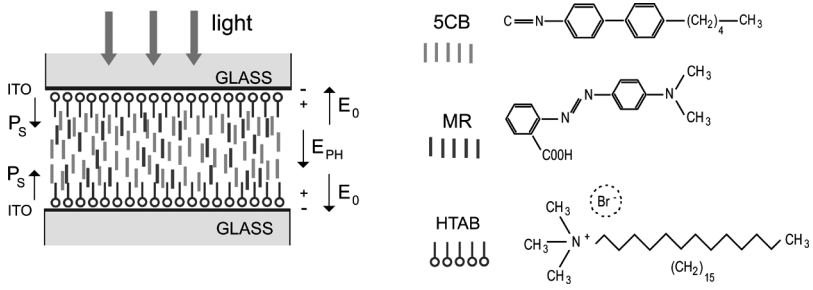

FIGURE 1 Schematic drawing of the LC cell, together with the chemical representation of the liquid crystal molecules (5CB), the azo-dyes (MR) and the surfactant (*HTAB*). The surface polarization, P_s, the surface charge electric field, E_0, and the photo-induced field, E_{PH}, are indicated close to the cell walls.

by observing the sample under a polarizing microscope. The cell prepared with $n = 19$ and 21 have shown perfect homeotropic orientation a few minutes just after the filling. On the contrary, the cell treated with $n = 17$, 15 and 13 have shown anchoring instabilities, that appear as transitions from planar to homeotropic alignment taking place on long time scale (hours or days) and on different areas of the treated surfaces.

In Figure 2, we display a few typical pictures taken at the microscope for a cell treated with $n = 1\,5$. In Figure 2a the interface between two differently oriented regions, planar (P) and homeotropic (H), respectively, can be clearly distinguished. The interface is strongly influenced by the light; it remains stable if the cell is kept in the dark but it becomes unstable when the cell is illuminated. By keeping the cell under the light of the microscope, we see the following sequence: at the beginning the interface becomes undulated (Fig. 2b); then, several domains with homeotropic orientation nucleate inside the planar region (Fig. 2c); and finally, small planar domains nucleate inside the homeotropic ones (Fig. 2d). When the cell is brought back in the dark, it takes several hours to recover the initial configuration with the stable and linear interface.

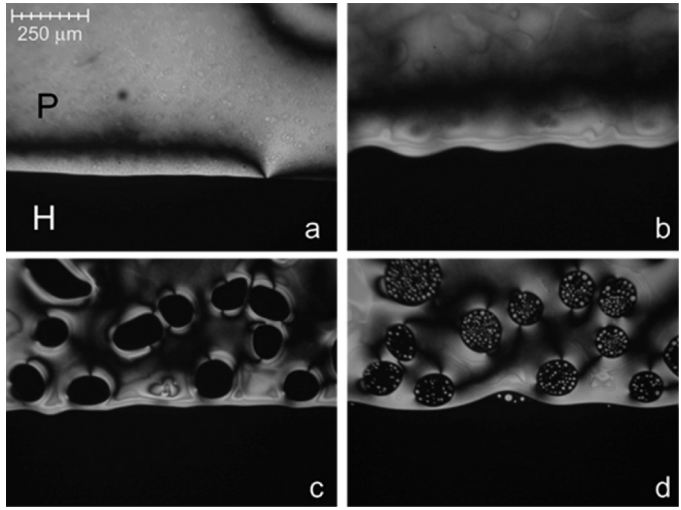

FIGURE 2 Alignment instability in a cell treated with C_{15}. The interface between the planar (P) and the homeotropic (H) anchoring at a) the beginning of illumination, b) after 1 minute, c) after 5 minutes and d) after 10 minutes under microscope illumination.

THE LIGHT INDUCED REORIENTATION

Experimental Setup

The experimental setup is shown in Figure 3. The liquid crystal cell is placed at the intersection of two linearly s-polarized, enlarged and collimated Ar^+ laser beams ($\lambda = 514\,\text{nm}$, s-polarization, beam diameter 5 mm). The angle between the two beams is $\alpha \simeq 1^\circ$, corresponding to a fringe spacing of $\Lambda \simeq 18\,\mu\text{m}$. The two Ar^+ beams propagates in the $x-z$ plane and are at normal incidence, that is, are symmetrically placed with respect to the normal of the cell. A linearly p-polarized 0.8 mW He-Ne laser is used to probe the grating. A typical diffraction pattern is shown in Figure 3. At the $+1$ and -1 diffraction order, a photodiode is placed to measure the intensity $I_{\pm 1}$, respectively.

When the pump beams are sent onto the cell, we observe a signal rising on both photo-diodes. In the Raman-Nath regime, $\Lambda^2 >> \lambda d$, the grating diffraction efficiency η is given by [10]

$$\eta = \left(\frac{\pi \Delta n d}{\lambda}\right)^2.$$

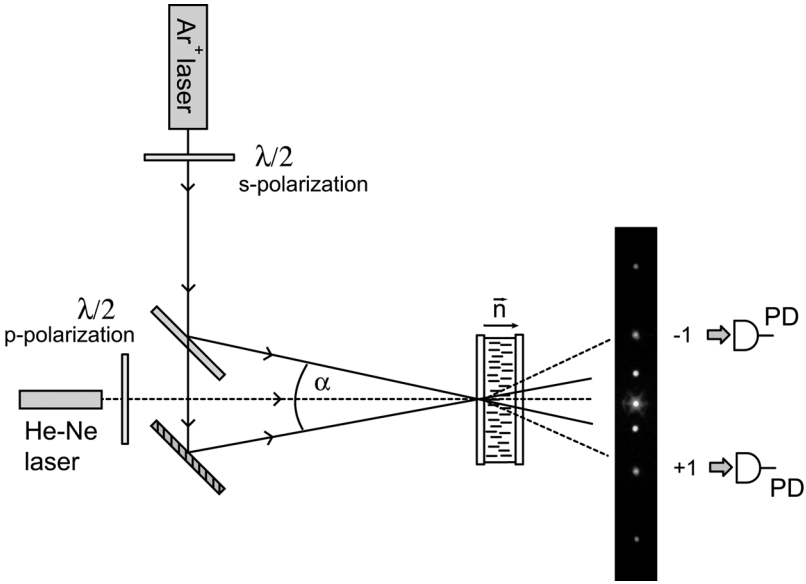

FIGURE 3 Experimental setup: $\vec{n}$ is the liquid crystal nematic director, $\lambda/2$ are half-wave plates. A typical diffraction pattern is shown at the exit of the cell, before the two photo-diodes (PD).

By measuring $\eta_{\pm 1} = I_{\pm 1}/I_0$ as the ratio between the intensity $I_{\pm 1}$ of the first order of diffraction and the total intensity I_0 of the probe beam, we obtain the value of n_2, characterizing the nonlinear optical response of the cell [11]:

$$\Delta n = n_2 I_{in},$$

where I_{in} is the total pump intensity incident on the cell.

Characterization at Different Lengths *n* of the C_nTAB Surfactant

We have performed several diffraction experiments by using homeotropic cells treated with C_nTAB and for different molecular length n. Typical recordings of the diffraction efficiency obtained are shown in Figure 4. The total intensity I_{in} of the two pumps vary in between 2.5 and 20 mW/cm^2.

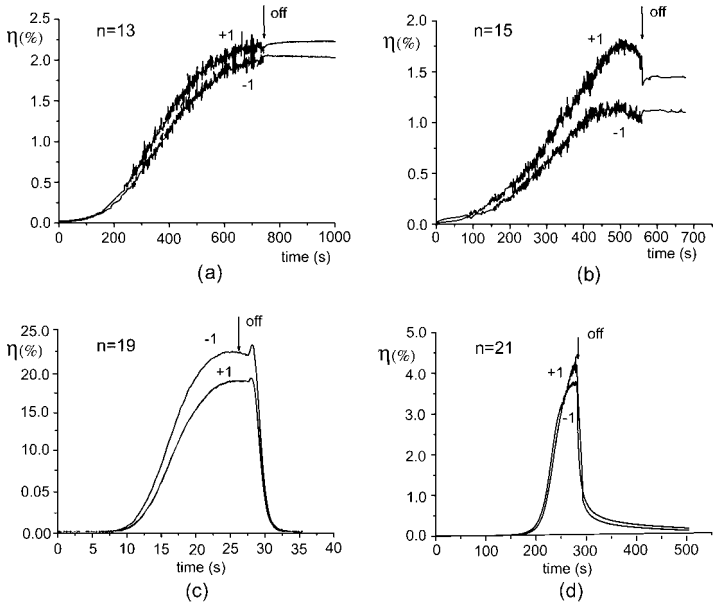

FIGURE 4 Diffraction efficiency as a function of time measured for a) $n = 13$ and $I_{in} = 5\,\text{mW/cm}^2$, b) $n = 15$ and $I_{in} = 5\,\text{mW/cm}^2$, c) $n = 19$ and $I_{in} = 1.0$ mW/cm^2, d) $n = 21$ and $I_{in} = 20\,\text{mW/cm}^2$. The arrows indicate the points where the pump beams were switched off.

The response time, as well as the diffraction efficiency of each cell, change with n. For $n = 13$,15 and 21 the response time is quite large and we have to wait approximatively one hundred seconds before the appearance of the first diffracted orders (Fig. 4a,b and d). For $n = 19$, the cells show a very high sensitivity for low input intensity and a relatively short (a few seconds) rising time (Fig. 4c). Once the grating is developed, the diffraction efficiency remains low for $n = 13$, 15 and 21 (Fig. 4a,b et d) while it grows up to 22% for $n = 19$ (Fig. 4c). Note that in the Raman-Nath regime the maximum diffraction efficiency for the first order cannot exceed 34% [10]. Memory effects are observed for $n = 13$, 15, that is, once written the grating becomes permanent and the diffraction persists even when the two pump beams are switched off. On the contrary, for $n = 21$ the response time is large but the writing procedure is reversible, that is, the grating disappears when the pumps are switched off.

For each cell, by taking the maximum value of the diffraction efficiency η_{+1} we calculate the nonlinear coefficient n_2 (similar results are obtained by using the values for η_{-1}). Then, we evaluate the time T needed to attain the 10% of maximum η_{+1}. In Figure 5, we report the values of n_2 and T obtained for the different cells, together with the different alignments obtained just after the filling. The maximum n_2 and the shortest T are obtained for $n = 19$, which is largely more sensitive and more efficient than the other cells. These experimental observations put into evidence the fundamental role played by the microscopic details at the interface between the liquid crystals and the surfactant used as anchoring agent. Indeed, the molecular length

n	Planar	Homeotropic	n_2 (cm^2/W)	T (sec)
13	X ⟷	X	0.40	180
15	X ⟷	X	0.40	130
17	X ⟷	X		
17 - 10 min		X	0.85	20
17 - 20 min		X	0.85	300
19		X	**6.70**	**6.5**
21		X	0.15	200

FIGURE 5 Table resuming the behaviors of the cells treated with C_nTAB for different n.

of the monolayer deposited onto the glass plates is of essential importance in determining the giant nonlinear response of the cell.

As a further validation for the existence of an optimal surfactant molecular length, we have studied in more detail the case of $C_{17}TAB$, that has a chain length closest to the optimal one. We have prepared two cells by keeping the glass plates in the surfactant solutions for a longer time with respect to the others (10 and 20 minutes). In this way, we simulate an effective lengthening of the surfactant chains, since more than a single molecular layer would be deposited on the surface. For both the 10 and the 20 minutes cells, the alignment becomes perfectly homeotropic a few minutes after the filling. The 10 minutes cell shows the same response time as for the $C_{19}TAB$, but n_2 is not as large (see Fig. 5). On the contrary, for the 20 minutes cell the optical response becomes very similar to that of the cell treated with $C_{21}TAB$, that is, very slow and not very efficient.

Characterization at Different MR Concentrations

One of the main features of the azo-dyes is that, under the action of light, they can change their molecular conformation. The process is called photoisomerization, and the two isomers are called, respectively, the *trans* and *cis* form [6]. In the *trans* state the MR molecules are more rod-like and aligned, in average, in the same direction as the surrounding liquid crystals, while in the *cis* state they are more isotropic and insensitive to the alignment of the surrounding liquid crystals. During the photoisomerization, by absorbing a photon, MR molecules go from the *trans* state to *the* cis one. Then, thermal relaxation brings them back to the trans form. These changes of molecular configuration help the reorientation of the liquid crystals, then increasing the optical response of the cell [12].

We have repeated the diffraction experiments by using *HTAB* treated cells and by changing the dye concentrations from $c = 0.1\%$ to 1.0%. For different MR concentrations, the cell absorption has been measured by using a commercial spectrometer (Ocean Optics UV-VIS 2000). The results are plotted in Figure 6, where the transmission coefficients T (at $\lambda = 514\,\text{nm}$) are normalized to 1 with respect to the transmission of a cell filled with a pure liquid crystal and of the same thickness ($d = 14\,\mu\text{m}$).

At low MR concentrations, such as $c = 0.1\%$, low intensities would show nothing and diffraction does not appear until around $0.6\,\text{mW/cm}^2$. However, after getting a signal with the higher intensities, the same cell showed a response even at lower intensities and a diffraction pattern would start to appear. The origin of this memory

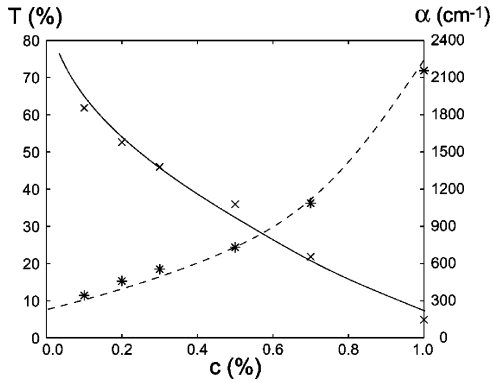

FIGURE 6 Cell transmission $T(\%)$ and absorption coefficient $\alpha(\mathrm{cm}^{-1})$ at $\lambda = 514\,\mathrm{nm}$ and for different dye concentrations.

effect has to be related to the induced photovoltaic effect. At the early times of illumination, only a few MR molecules are excited and in the same time those molecules are uniformly distributed in the volume. Because of the photovoltaic effect, and the associated field E_{PH}, the MR molecules start to move towards the surface of the confining ITO coated plates (see Fig. 1). By keeping the laser onto the cell, the more and more MR molecules get excited and go close to the surface. Eventually, at high laser intensity, MR molecules can bind chemically to the surfactant molecules, leading to the formation of permanent gratings [13].

When the laser is shone onto the cell for a second time, less energy is needed to stir the MR molecules as some have already moved, and so already being excited, start to create an easy axis at the surface. For higher concentrations of the dye, such as $c = 0.5\%$, responses could be obtained at lower intensities, of the order of $50\,\mu\mathrm{W/cm}^2$. However, this had the consequence of starting to diffuse light at lower input intensities. Indeed, when the MR concentration increases, or the pump intensity is high, the molecular reorientation becomes irregular and characterized by large fluctuations. In Figure 7a and b it is shown a diffraction pattern observed for $c = 0.5\%$ at low, $I_{in} = 150\,\mu\mathrm{W/cm}^2$, and high, $I_{in} = 1.5\,\mathrm{mW/cm}^2$, pump intensity, respectively. For high values of I_{in} the refractive index grating becomes unstable and a large light scattering appears in all directions. Large director fluctuations have been observed also for the self diffraction induced by illuminating the cell with two circularly polarized pumps, both in the same directions [14].

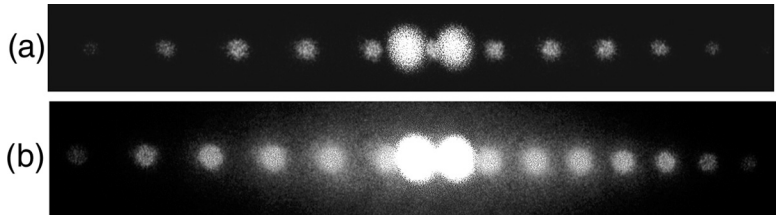

FIGURE 7 Probe diffraction for a *HT AB* treated cell filled with a MR concentration $c = 0.5\%$: a) $I_{in} = 150\,\mu W/cm^2$ and b) $I_{in} = 1.5\,mW/cm^2$.

Note that the *cis–trans* relaxation process may be either a thermal one either a photo-induced transition. At relatively high values of MR concentrations, the absorption of the probe beam ($\lambda = 633\,nm$) may become sufficiently large to induce a significant role of the *cis–trans* photo-induced transition [15]. A transmission spectrum of a $c = 0.5\%$ dye-doped cell is shown in Figure 8, where a small dip may be distinguished around the wavelength of the probe beam.

For a fixed concentration, $c = 0.1\%$, 0.5% and 1.0%, we varied the pump intensity, we measured the diffraction efficiency and we evaluated the nonlinear coefficient n_2. In Figure 9a the values of n_2 are plotted against the pump intensity. For each different dye concentration, a dashed line marks the value of the input intensity at which a diffraction pattern is distinguishable at the first times of the cell illumination. It can be noted that all the measured values of n_2 fit on the same curve, independently of the concentration. If we plot the inverse of n_2 as a function of I_{in}, as in Figure 9b, we can see that all the points scale linearly with the input intensity. This means that the sensitivity of the cell does indeed not depend on the input pump intensity, since saturation has been reached for any value of I_{in}. On the other side, varying the dye concentration only changes the

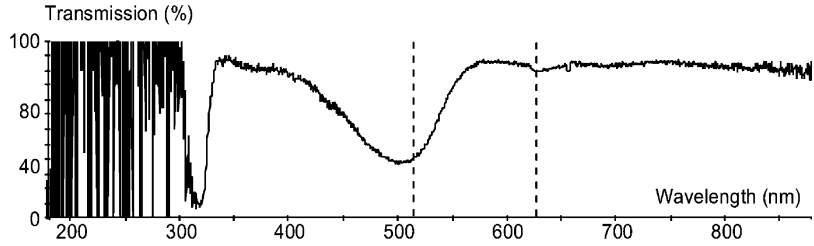

FIGURE 8 Transmission spectrum of a $c = 0.5\%$ dye-doped cell. Dashed lines mark the wavelength of the pump (514 nm) and that of the probe (633 nm).

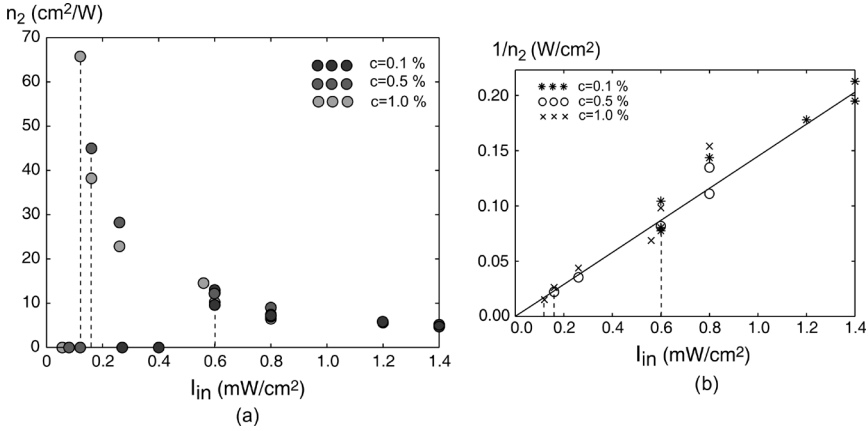

FIGURE 9 a) Nonlinear coefficient and b) its inverse as a function of I_{in}. The straight line in b) is a linear fit with a slope 0.145. For each concentration, a dashed line marks the values at which a diffraction signal starts to be distinguishable.

start-up point but does not alter the slope of the line on which fit all the data. This means that, above a certain value of minimal dye concentration, such as $c = 0.1\%$, the cell sensitivity is not affected by the dye concentration and the maximum photo-induced birefringence, $\Delta n = n_2 I_{in}$, is constant.

Interpretation of the Results

A qualitative explanation of the observed phenomena can be given starting from some considerations on the mechanisms involved in the anchoring process. In the determination of the effective anchoring energy, W_{eff}, we have to include the anchoring force $W_0 \propto (\vec{n} \cdot \vec{n}_0)^2$ imposed by the easy-axis $\vec{n}_0$ on the surface, plus a term proportional to $(\vec{E}_0 \cdot \vec{n})^2$, where $|\vec{E}_0| = \sigma / < \varepsilon > \varepsilon_0$ is the electric field generated by the surface charge density σ, ε_0 is the vacuum permittivity and $< \varepsilon > = (\varepsilon_\parallel + 2\varepsilon_\perp)/3$, $\varepsilon_\parallel$ and $\varepsilon_\perp$ being the dielectric constants parallel and orthogonal to $\vec{n}$, respectively. In general, it must also be included a term of surface polarization, $(\vec{P}_s \cdot \vec{E}_0)$, that arises as a consequence of any symmetry breaking present at the surface. When considering all these contributions, W_{eff} becomes a function of the surface charge density σ [16,17] :

$$W_{eff} = W_0 + \alpha_1(\lambda_D)\sigma^2 + \alpha_2(\lambda_D, \lambda_s)\sigma$$

where the coefficients α_1 and α_2 depend on the Debye screening length for the electric field $\vec{E}_0$, $\lambda_D \sim 600\,\text{nm}$, and on the screening length for the surface polarization $\vec{P}_s$, $\lambda_s \sim 10\,\text{nm}$. The other typical length scale involved is the thickness of the surfactant monolayer, that corresponds to a single molecular length, about 26 Å for the *HTAB* [18]. This length changes by changing the number n of CH_2 groups. This can alter the surfactant adsorption properties at the glass surface as well as its solubility in the water.

From the above expression, we see that W_{eff} may have a minimum for a certain value of σ. In this case, changing the surface charge density may lead to a change of the anchoring energy and eventually to the transition from the homeotropic to the planar alignment [17]. Indeed, it is already known that changing the surface charge density can change the anchoring energy and induce transitions from planar to homeotropic alignment [16]. Thus, the anchoring instabilities that we have observed for short chain lengths under the microscope illumination can be explained if we consider that, under illumination, the photo-induced voltage E_{PH} can induce a change of σ. The existence of a critical chain length that optimizes the optical response should be related to the fact that this length minimizes the anchoring energy and thus renders the system more sensitive to the photo-induced changes.

Moreover, it has been recently shown that the photoisomerization of the azo-dyes close to the surface can also alter σ [19], thus contributing to the modulation of W_{eff}. As we have discussed in relation with the experiments at different dye concentrations, when the light is shone onto the cell, the photo-induced field E_{PH} pushes the MR molecules towards the surface of the cell, where their photoisomerization can be effective in modulating the surface charge density and, hence, the anchoring energy. A more detailed, and eventually quantitative, explanation of the phenomenon would require a careful comparison of all the relevant length scales, comprised the surface roughness, and all the involved energies, comprised the adsorption of the surfactant molecules at the surface.

POLARIZATION HOLOGRAPHY

As further investigations about the mechanisms generating light-induced re-orientational phenomena in azo-dye doped nematics, we have studied the response of the cells by using a polarization holographic technique. Polarization interference patterns are obtained by superposing two orthogonally polarized beams. The polarization of each pump beam is controlled by a quarter-wave or a half-wave

plate, in such a way to fix orthogonal polarizations. The interference polarization pattern has a spatial period $\Lambda \approx 17\,\mu\text{m}$, so that the Raman-Nath condition, $\Lambda^2 >> \lambda d$, is fulfilled. Two types of polarization patterns were used in the experiment, as listed below.

Left and right circularly polarized pumps. By using two quarter-wave plates, right and left circularly polarized incident beams are obtained. The superposition of the two beams creates an optical field which can be written in the form:

$$\vec{E}_{opt} \propto \hat{x}\cos\left(\frac{1}{2}\vec{K}\cdot\vec{r}\right) + \hat{y}\sin\left(\frac{1}{2}\vec{K}\cdot\vec{r}\right) \tag{1}$$

where $\vec{x}$ and $\vec{y}$ are unit vectors along the p-polarized and the s-polarized state, respectively, and $\vec{K}$ is the grating vector, $K = 2\pi/\Lambda$. As shown in Figure 10a, the polarization state is everywhere linear and goes through vertical, $+45^\circ$, horizontal, -45° and back to vertical in one period.

$\pm 45^\circ$ linearly polarized pumps. By using two half-wave plates, pump beams linearly polarized at $+45^\circ$ and -45°, respectively, are obtained. The interference of the two beams produces an optical field which can be written in the form:

$$\vec{E}_{opt} \propto \hat{x}\cos\left(\frac{1}{2}\vec{K}\cdot\vec{r}\right) + i\hat{y}\sin\left(\frac{1}{2}\vec{K}\cdot\vec{r}\right) \tag{2}$$

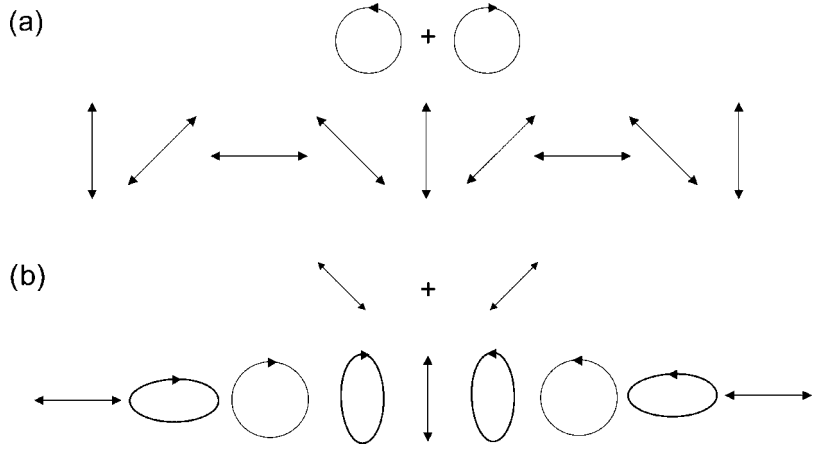

FIGURE 10 Polarization patterns obtained through the interference of a) left and right circularly polarized pumps, b) $\pm 45^\circ$ linearly polarized pumps.

where $i = \sqrt{-1}$. As shown in Figure 10b, the polarization state varies from linear horizontal, right circular, linear vertical, left circular and back to linear horizontal in one period, passing through elliptical polarization states.

As usual, the occurrence of a diffraction grating inside the cell is tested by a low power (0.8 mW) He-Ne laser ($\lambda = 633$ nm), used as probe beam. The probe beam is at normal incidence on the sample and its polarization is fixed by using a half-wave or a quarter-wave plate. The quality of the diffraction grating is evaluated by measuring the diffraction efficiency, $\eta_{\pm 1} = I_{\pm 1}/I_0$.

For left and right circularly polarized pumps, dynamical diffraction gratings are observed and typical rise time is about 100 sec. The diffraction efficiency of the grating depends on the state of polarization of the probe beam. In Figure 11 the time evolution of $\eta_{\pm 1}$ are reported for linear a) s and b) p-polarization of the probe as well as for c) left and d) right circular probe polarization. For all measurements the total pump intensity is $I_{in} = 2\,\mathrm{mW/cm^2}$. At the beginning of the grating formation, $\eta_{\pm 1}$ have the same value in the case of linear probe, while for circular probe only the $+1$ or -1 diffracted order is present

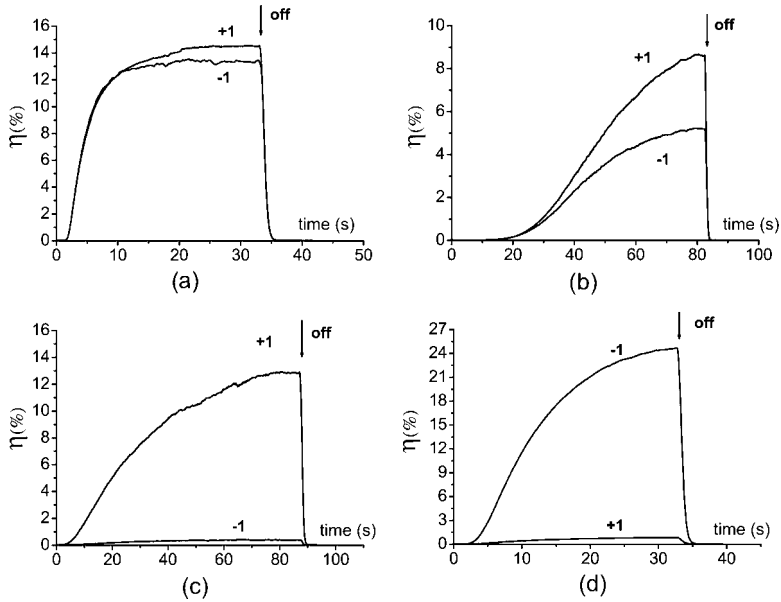

FIGURE 11 Time evolution of the diffraction efficiencies $\eta_{\pm 1}$ in the case of a) linear s, b) linear p, c) left circular and d) right circular probe. Pump intensity is $I_{in} = 2\,\mathrm{mW/cm^2}$.

for left or right circular polarization, respectively. At longer times, when saturation takes place, the response of the grating changes. For linear probe a separation in the values of η_{+1} and η_{-1} appears. This separation is much larger for the p-polarized probe than for the s-polarized one. Besides, in the case of left (right) circular probe, the -1 ($+1$) diffracted order, that was not present at the beginning of the grating formation, also appears (see Fig. 11c and d, respectively). When the pump beams are switched off, the grating is completely erased, at variance with previously reported experiments for planar cells [7]. The maximum diffraction efficiency, $\eta_{-1} \sim 24\%$, is obtained for right circular probe, whereas $\eta_{+1} \sim 14\%$ for left circular probe.

From the temporal evolution of $\eta_{\pm 1}$ we see that, during the grating buildup, the director reorientation exactly follows the local electric field along the polarization pattern. This leads to a diffraction grating corresponding to the ideal case, for which the diffracted $+1$ and -1 orders are expected to have opposite circular polarizations and the grating separates any incident polarization into two circular orthogonal components [20]. Thus, for a linear probe, the intensities of the $+1$ and -1 diffracted orders should have the same value, $\eta_{+1} = \eta_{-1} = (\sin^2 \Delta\phi)/2$, where $\Delta\phi = (2\pi/\lambda)\,\Delta n d$ and Δn is the photo-induced birefringence. In the case of a circularly polarized probe, only one diffracted beam is expected. For a left circular probe $\eta_{-1} = 0$ and $\eta_{+1} = \sin^2 \Delta\phi$, while for a right circular probe $\eta_{+1} = 0$ and $\eta_{-1} = \sin^2 \Delta\phi$. We see from Figure 11 that these rules are respected during the grating build-up, until saturation of the reorientation takes place.

The observed behaviors can be qualitatively explained by considering that surface effects play a fundamental role at the beginning of the reorientation [4]. Thus, *trans-cis* photoisomerization of the dye close to the first surface of the cell (illuminated side) triggers the light-induced weakening of the anchoring condition and the subsequent reorientation of the LC molecules. During the grating buildup, the director reorientation, driven by this surface effect, follows the direction imposed by the polarization pattern. Later, the reorientation is transferred in the volume of the cell, where bulk effects become important. Here, slight distortions with respect to the ideal case appear because of the elastic coupling with the other surface of the cell.

As further tests, we have measured the steady-state values of the diffraction efficiencies $\eta_{\pm 1}$ by gradually varying the polarization state of the probe. At this purpose, a quarter-wave plate on the probe beam is put in rotation at a constant speed by using a motorized rotation stage. This way, all polarization states are realized, depending on

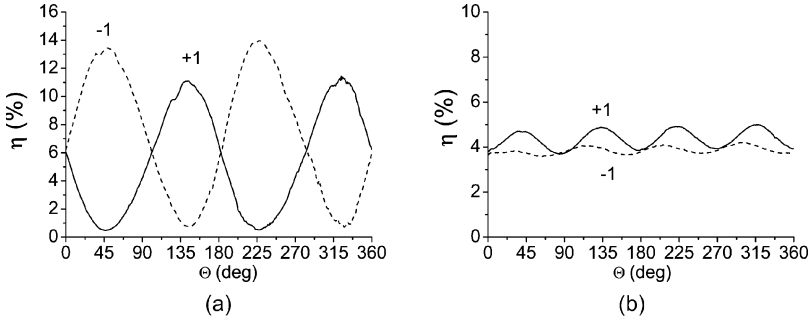

FIGURE 12 Diffraction efficiencies $\eta_{\pm 1}$ vs Θ; Θ is the angle between the probe polarization and the fast axis of a) the quarter-wave plate and b) the half-wave plate.

the angle Θ between the fast axis of the quarter-wave plate and the polarization of the probe chosen as reference (s-polarization). As shown in Figure 12a, for circularly polarized probe ($\Theta = (2n + 1)\,45^\circ$, $n = 0, 1, 2, \ldots$) only one diffracted beam prevails, while the other one can be neglected. For linearly polarized probe ($\Theta = n\,90^\circ$, $n = 0, 1, 2, \ldots$), η_{+1} and η_{-1} have the same value, though a weak separation is more evident for the p-polarized probe ($\Theta = 90^\circ$ and 270°) than for the s-polarized one ($\Theta = 0^\circ$ and $\Theta = 180^\circ$). For intermediate states of polarization, the $+1$ and -1 diffracted orders are proportional to the left and right circular polarization components into which the probe can be decomposed. We have repeated the same experiment by using a half-wave plate on the probe beam. This way, all linear polarization states are realized, depending on the angle Θ between the fast axis of the half-wave plate and the s-polarization of the probe. In this case, we expect η_{+1} and η_{-1} to have the same value, independently from the linear probe polarization. However, as shown in Figure 12b, a separation in η_{+1} and η_{-1} occurs. This separation is almost zero in the case of s-polarization ($\Theta = n\,90^\circ, n = 0, 1, 2, \ldots$) whereas it is maximum in the case of p-polarization ($\Theta = (2n + 1)\,45^\circ, n = 0, 1, 2, \ldots$).

When the pump beams are $\pm 45^\circ$ linearly polarized, dynamical diffraction gratings also appear with a typical time scale of 100 seconds and the diffraction efficiency depends on the state of polarization of the probe beam, as shown in Figure 13. Nevertheless, in this case the response of the grating significantly differs with respect to the ideal behavior. Indeed, in this case η_{+1} and η_{-1} are expected to be independent on the polarization of the probe and to have the same

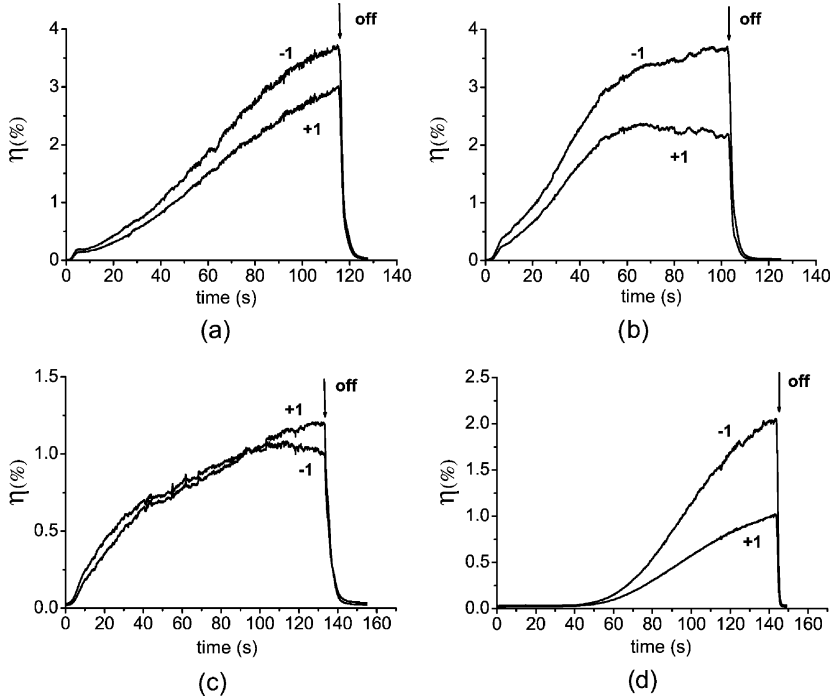

FIGURE 13 Time evolution of the diffraction efficiencies $\eta_{\pm 1}$ in the case of a) linear s, b) linear p, c) left circular and d) right circular probe. Pump intensity is $I_{in} = 8\,\mathrm{mW/cm^2}$.

value, that is, $\eta_{+1} = \eta_{-1} = |J_1(\Delta\phi)|^2$, where $J_1(\Delta\phi)$ is the first order Bessel function [21]. Moreover, for the diffracted waves, the grating should act as a half-wave plate with the fast axis at 45° from the vertical direction.

The experimental results show that for linear probe (Fig. 13a and b) a separation in the η_{+1} and η_{-1} values is always present. For left circular probe (Fig. 13c) the $+1$ and -1 diffracted orders reach the same steady-state value and substantially there is no separation until saturation. On the contrary, for right circular probe η_{+1} and η_{-1} are always different and $\eta{-}1$ reaches a higher value with respect to η_{+1} (Fig. 13d). When the pump beams are switched off the grating is completely erased. The maximum diffraction efficiency, $\eta_{-1} \sim 3.5\%$, is obtained for s or p-polarized probe. This value is much smaller than the maximum diffraction efficiency obtained for circularly polarized pumps. For any probe polarization the $+1$ and -1 diffracted orders

are elliptically polarized and a strong light diffusion is observed, showing that the molecular director is not fixed in one direction, but it is rather fluctuating between different orientations, compatible with the mixed states along the polarization pattern.

We have also tested the diffraction gratings by gradually varying the polarization state of the probe, through rotation of a quarter-wave plate. We observe a strong dependence of $\eta_{\pm 1}$ from the probe polarization and a higher separation in the η_{+1} and η_{-1} values for circular probe with respect to linear probe. By rotating a half-wave plate, we observe that the separation of η_{+1} and η_{-1} remains almost constant for any linear polarization.

From these observations, we can conclude that the diffraction gratings obtained by the interference of $\pm 45^\circ$ linearly polarized pumps are less efficient than those obtained by opposite circularly polarized pumps. Moreover, their response considerably differs with respect to the ideal case. A possible explanation of this difference can be found by considering the behavior of the molecular reorientation in the circularly polarized regions. Since in the absence of any symmetry breaking there is no preferential orientation for the director reorientation, we would expect that in these regions the molecular director is randomly distributed. However, it has been shown that, in the case of two circularly polarized pumps, both in the same direction, the reorientation of the nematic director follows a three-dimensional trajectory that is strongly influenced by a weak symmetry breaking related to the treatment of the cell surfaces [14]. This symmetry breaking is introduced by the direction of withdrawing of the glass plates during the deposition of the anchoring agent. In our case, as the cell preparation is the same, we can assume that in the circularly polarized regions, the director, instead of being randomly distributed, reorient along the direction of the symmetry breaking. This effect is not very important in the case of opposite circularly polarized pumps, since the linear polarization along the interference pattern always dominates the molecular reorientation, thus imposing a specific direction. However, the observed small separation between η_{+1} and η_{-1}, as well the slight asymmetry between the s and p-polarized probe, may be attributed to the same influence of the withdrawing direction.

CONCLUSIONS

We have presented new advancements in the understanding the origin of the giant nonlinear optical response in azo-dye doped nematics. We have changed the surface anchoring conditions by varying the length n of the aliphatic chain of the C_nTAB surfactant. We have shown that an

extremely high response is obtained only in the case $n = 19$, corresponding to *HTAB*, a product already known as a liquid crystal anchoring agent [9]. We have changed the dye concentration and we have tested the cells in different experimental geometries, either for linear or circular polarization of the pumps. All the results give indications that the extremely high sensitivity of azo-dye doped nematics is not only strongly related to the presence of ionic surfactant on the side-walls of the cell, but is even strongly influenced by the molecular conformation of the surfactant.

By illuminating the cells with two pump beams both circularly polarized in the same direction, we have previously shown that the motion of the nematic director is characterized by a relatively fast in-plane component followed by a much slower and out-of plane component [14]. Here, we have reported dynamical diffraction gratings arising when the cell is illuminated by two pumps beams polarized in opposite directions, either circularly or linearly. The resulting interference pattern has a uniform intensity, whereas the local polarization varies periodically in space. As no intensity modulation is present in the interference region, the occurrence of a diffraction grating inside the cell shows that the light induced reorientation of the liquid crystal molecules is the main effect, and allows to neglect all the mechanisms related to light intensity gradients, such as charge migration or thermal heating.

During the grating build-up, the molecular reorientation exactly follows the direction of the electric field along the polarization pattern. This is true especially for left and right circularly polarized pumps. In this case the diffraction gratings decompose any incident polarization into two opposite circular components. This property has been widely investigated in azobenzene materials, such as side-chain azobenzene polymers and azo-dye guest-host polymers [22,23], in which permanent diffraction gratings are recorded through the light induced reorientation of the azobenzene chromophores. Polarimetric applications of this property have also been proposed [24]. On the contrary, in the case of $\pm 45^\circ$ linearly polarized pumps, the grating dynamics significantly differs with respect to the ideal case. This difference could be related to a slight symmetry breaking in the sample, such as the influence of the withdrawing direction during the cell preparation.

In summary, we can conclude that the light induced molecular reorientation in azo-dye doped cells results as a combination of the surface effect with the bulk features of the MR molecules. The reorientation starts at the surface, because of the migration and excitation of the MR molecules close to the confining plate, and then propagates in the bulk. As the surface-induced reorientation sets in, dye-doped

liquid crystals begin to absorb more and more light because of the dye dichroism and the diffraction signal grows with a long time scale. This slow process is accompanied by the *trans–cis* photoisomerization of the dye molecules and saturates after a time that decreases with increasing the input light intensity [3]. Memory effects are related to the induced photovoltaic effect and may become important either at high input intensity or at relatively high values of MR concentrations, eventually leading to the recording of permanent gratings. Here, dynamical gratings have been proved to arise under illumination with polarization patterns. The observed optical properties are promising for photonic applications, such as dynamical optical memories and polarimetric devices.

The reported measurements confirm the extremely high sensitivity of the azo-dye doped nematics and shed light onto the microscopic mechanisms that are at the origin of their "supranonlinear" optical response.

REFERENCES

[1] Khoo, I. C., Slussarenko, S., Guenther, B. D., Shih, M.-Y., Chen, P., & Wood, W. V. (1998). *Opt. Lett.*, *23*, 253.
[2] Simoni, F., Lucchetti, L., Lucchetta, D. E., & Francescangeli, O. (2001). *Optics Express*, *9*, 85.
[3] Petrossian, A. & Residori, S. (2002). *Europhys. Lett.*, *60*, 79–85.
[4] Residori, S. & Petrossian, A. (2003). *Mol. Cryst. Liq. Cryst.*, *1398*, 137–156.
[5] Lucchetti, L., Di Fabrizio, M., Francescangeli, O., & Simoni, F. (2004). *Optics Commun.*, *233*, 417–424.
[6] Gibbons, W. M., Paul J., Shannon, Shao-Tang Sun, & Swetlin, B. J. (1991). *Nature*, *351*, 49–50.
[7] Slussarenko, S., Francescangeli, O., Simoni, F., & Reznikov, Y. (1997). *Appl. Phys. Lett.*, *71*, 3613.
[8] Shishido, A., Shih, M.-Y., Khoo, I. C. (2002). *J. Nonlin. Opt. Mater.*, *11*, 1.
[9] Cognard, J. (1982). *Mol. Cryst. Liq. Cryst. Suppl. Ser. 1*, 1.
[10] Yariv, Y. & Yeh, P. (2003). *Optical waves in crystals*, John Wiley and Sons, Inc., Hoboken, New Jersey.
[11] Tabiryan, N. V., Sukhov A. V., & Ya. Zel'dovich, B. (1986). *Mol. Cryst. Liq. Cryst. 136*, 1.
[12] Voloschenko, D., Khyzhnyak, A., Reznikov, Y., & Reshetnyak, V. (1995). *Jpn. J. Appl. Phys. 34*, 566.
[13] Voloschenko, D. & Lavrentovich, O. D. (1999). *J. Appl. Phys. 86*, 4843.
[14] Petrossian, A. & Residori, S. (2003). *Opt. Commun. 228*, 145, (2003).
[15] Lee, C. R., Mo, T. S., Cheng, K. T., Fu, T. L., & Fuh, A. Y. G. (2003). *Appl. Phys. Lett. 83*, 4285.
[16] Zakharov, A. V. & Dong, R. Y. (2001). *Phys. Rev. E* 64, 042701.
[17] Kunhnau, U., Petrov, A. G., Klose, G., & Schmiedel, H. (1999). *Phys. Rev. E 59*, 578.
[18] Fragneto, G., Thomas, R. K., Rennie, A. R., & Penfold, J. (1996). *Langmuir 12*, 6036.

[19] Zakharov, A. V. & Iwamoto, M. (2003). *J. Chem. Phys. 118*, 10758.
[20] Nikolova, L., & Todorov, T. (1984). *Opt. Acta 31*, 579.
[21] Nikolova, L., Todorov, T., Ivanov, M., Andreuzzi, F., Hvilsted, S., & Ramanujam, P. S. (1996). *Appl. Optics 35*, 3835.
[22] Naydenova, I., Nikolova, L., Todorov, T., Holme, N. C. R., Hvilsted, S., & Ramanujam, P. S. (1998). *J. Opt. Soc. Am. B 15*, 1257.
[23] Nikolova, L., Nedelchev, L., Todorov, T., Petrova, Tz., Tomova, N., Dragostinova, V., Hvilsted, S., & Ramanujam, P. S. (2000). *Appl. Phys. Lett. 77*, 657.
[24] Cipparrone, G., Mazzulla, A., & Blinov, L. M. (2002). *J. Opt. Soc. Am. B 19*, 1157.